Ship Wake Detectability in TerraSAR-X, CosmoSkymed, Sentinel-1 and RADARSAT-2 Imagery – Summary and Applications for Wake Detection

Björn Tings[a], Andrey Pleskachevsky[a], Stefan Wiehle[a], Sven Jacobsen[a]
[a] DLR, Maritime Safety and Security Lab Bremen, Am Fallturm 9, 28359 Bremen, Germany
Bjoern.Tings@dlr.de

1. Introduction

Ship wakes are produced by the interaction of the ship's hull with the ocean water and are result of multiple interacting wave systems closely beneath and on the ocean surface. The ship wake signatures in SAR imagery consists of various components. The most frequently encountered wake components are Kelvin wake arms, V-narrow wake arms and two parts of the turbulent wake: the near field and the far field [1]. The detectability of these four most important wake components in SAR imagery is influenced by several physical variables, which are in the following called influencing parameters. The influencing parameters can be categorized into ship properties, environmental conditions and SAR acquisition settings.

In a series of preceding studies of the authors [1, 2], the characteristics of the effects of influencing parameters on the detectability of individual wake components have been modelled using machine learning, categorized, and contrasted against the published state-of-the-art. For the latest study [3], the list of the satellites was extended and the detectability of wake components was investigated in terms of different radar frequency bands (C-Band and X-Band SAR) and different orbit altitudes (i.e. slant ranges).

This study summarizes the method and the results of the preceding studies [1,2,3] and the application of the results to the actual task of wake detection is demonstrated. The demonstration shows that the developed models can be applied to control the precision performance of wake detectors and to estimate vessel velocity with an accuracy coinciding with other published methods [4].

2. Materials and Method

The studies are based on four different SAR missions (Table 1). The ground truth wake samples listed for each sensor were created by a manual inspection procedure.

Table 1: Summary of wake component datasets

Sensor name	TerraSAR-X (TSX)	CosmoSkymed (CSK)	Sentinel-1 (S1)	RADARSAT-2 (RS2)
Frequency band /radar wavelength [cm]	X / 3.1	X / 3.1	C / 5.6	C / 5.6
Orbit-Altitude [km]	514	619	693	798
Approx. slant range [km] at 30°/50° incidence angle	593 / 800	715 / 963	800 / 1078	922 / 1242
Acquisition modes / product types	SL, SM / MGD	HIMAGE / DGM	IW / GRDH	MF, F, S / SGF
Number of total wake samples (HH / VV)	2881 (2429 / 452)	94 (94 / 0)	618 (0 / 618)	407 (407 / 0)

The detectability of each of the four wake components was modelled for each of the four sensors using the support vector regression (SVR) method. The length of each wake component is used as indicator for the wake component's detectability. The preceding studies have an intersecting set of five influencing parameters, which are listed in Table 2.

The SVR models predict which wake component lengths are expected depending to the conditions defined by the influencing parameters. The predicted wake component lengths are then linearly normalized between a minimum and maximum length boundary to obtain a measure of detectability with uniform scale. The so-called detectable length metric (DLM) for a sensor s and a wake component w is:

$$DLM_{w,s}(x_1, \dots, x_5) = \left(f_{w,s}(x_1, \dots, x_5) - l_w^{min}\right) / \left|l_w^{max} - l_w^{min}\right| \quad \text{(Eq. 1)}$$

where $x_1, \dots, x_5$ defines the five influencing parameters and $f_{w,s}$ the SVR model. l_w^{min} is the minimum length boundary and l_w^{max} maximum length boundary, both depending on the respective wake component.

The compositions of the created SVM models are analyzed and compared in order to derive statements on wake component detectability. A measure of the detectability models' uncertainty is provided to support the derived statements.

Table 2: List of the five influencing parameters with descriptions

Nr x_i	Parameter name	Description	Value range	
			x_i^{min}	x_i^{max}
x_1	AIS-Vessel-Velocity	Velocity of the vessel derived from AIS messages interpolated to the image acquisition time	1	10
x_2	AIS-Length	Length of the corresponding vessel based on AIS information	5	35
x_3	AIS-CoG	The Course over Ground (CoG) based on AIS information relative to the radar looking direction (0° means parallel to range, 90° mean parallel to Azimuth).	0	90
x_4	Incidence-Angle	Incidence angle of the radar cropped to TSX's full performance value range	20	45
x_5	SAR-Wind-Speed	Wind speed estimated from the SAR background around the vessel using the XMOD-2 (X-band) and CMOD-5 (C-band) geophysical model functions	2	9

The uncertainty measure quantifies, whether the models' compositions are learned systematically or randomly. The analysis is based on heatmaps as shown exemplarily in Figure 1. This example heatmap provides insight into the dependency of detectability of Kelvin wake arms on three influencing parameters describing ship properties [1, 2].

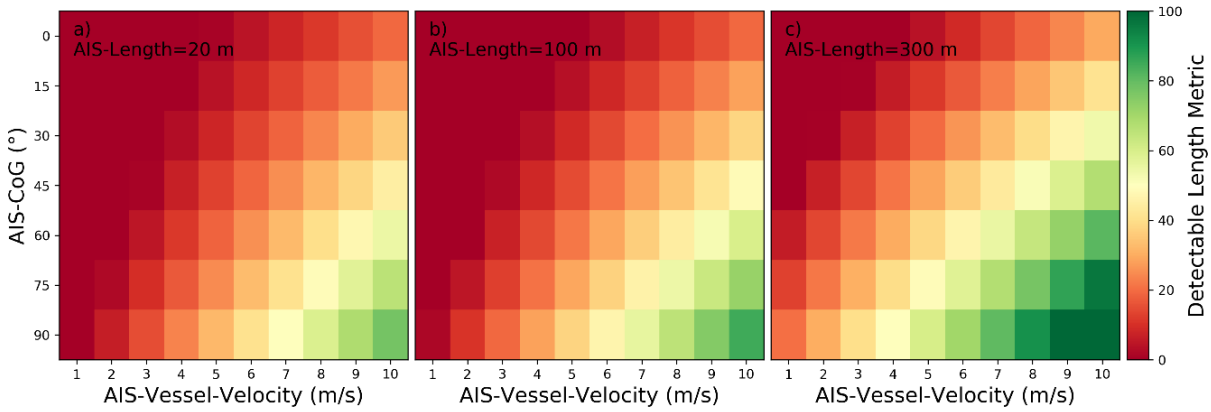

*Figure 1: Detectability heatmaps for accumulated port and starboard Kelvin wake arms based on AIS-Vessel-Velocity, AIS-CoG and from left to right AIS-Length with **a)** 20 m, **b)** 100 m, and **c)** 300 m.*

The comparison between models of two SAR sensors s_1 and s_2 is based on integrated differences in detectability [3]:

$$\overline{\Delta DLM_{w,s_1,s_2}} = \overline{DLM_{w,s_1}} - \overline{DLM_{w,s_2}} \quad \text{(Eq. 2)}$$

with

$$\overline{DLM_{w,s}} = \frac{1}{\Delta x_1 \dots \Delta x_5} \int \dots \int_V DLM_{w,s}(x_1, \dots, x_5)\ dx_1 \dots dx_5 \quad \text{(Eq. 3)}$$

where $\Delta x_i = x_i^{max} - x_i^{min}$ with $\left[x_i^{max}, x_i^{min}\right]$ is defined in Table 2. The multidimensional integration over the five-dimensional feature space is restricted by the volume $V = \left[x_1^{max}, x_1^{min}\right] \times \dots \times \left[x_5^{max}, x_5^{min}\right] \subseteq \mathbb{R}^5$.

3. Results

A summary of statements derived from studies [1, 2, 3] are summarized in Table 3. It should be noted that the statements from [1, 2] are revised in this study, as a measure for SVR models' uncertainties was developed in [3] and is additionally considered here.

4. Applications

The listed statements contribute primarily to the fundamental research of imaging and detection of ship wakes in SAR. The presented method for modelling of wake component detectability by SVR models, consequently and systematically takes all selected influencing parameters into account. Due to this completeness, a new opportunity of applying the detectability models to the task of wake detection arises. For

this purpose, a simple DeepLearning-based wake component detection system was developed. The applicability of the wake detectability models to wake detection is then demonstrated by two independent operations:

1. The sensitivity of wake detection systems can be controlled by the detectability models to increase precision while mainly maintaining the recall. The demonstration estimates that precision is increased by ~6% while recall only is decreased by ~3%
2. After detection of wake components by wake detection systems a reversion of the detectability models can be applied to estimate the ship velocity using the probability of detection PoD as substitute for $DLM_{w,s}\left|l_{w,s}^{max} - l_{w,s}^{min}\right| + l_{w,s}^{min}$ in reversed model:

$$f_{w,s}^{x_1\,-1}\left(DLM_{w,s}\left|l_{w,s}^{max} - l_{w,s}^{min}\right| + l_{w,s}^{min}, x_2, x_3, x_4, x_5\right) = x_1 \qquad \text{(Eq. 4)}$$

The demonstration estimates that the total error of this method is RMSE=2.71 m/s

Table 3: Summary on detectability of four wave components; identical influence marked by grey color

Influencing parameters	**Summary on detectability four wave components** **wake component detectability: "↑": better, "≈ ": hardly influenced**			
	near-hull turbulence	**turbulent wakes**	**Kelvin wake arms**	**V-narrow wake**
Vessel speed	↑ for faster moving vessels	↑ for faster moving vessels	↑ for faster moving vessels	↑ for faster moving vessels
Vessel length	↑ for larger vessels	↑ for larger vessels	↑ for larger vessels	↑ for larger vessels
Vessel moving direction	↑ for vessels moving parallel to range, when ship speeds are at most moderate	≈ (literature: ↑ for vessels moving parallel to azimuth, with low degree)	↑ for vessels moving parallel to azimuth	↑ for vessels moving parallel to azimuth
Incidence angle	↑ for larger incidence angles, when ship speeds are at least moderate	↑ for lower incidence angles	↑ for lower incidence angles	↑ for lower incidence angles
Local wind speed	↑ for lower wind speeds	↑ for lower wind speeds	↑ for lower wind speeds	↑ for lower wind speeds
Sea state wave height	≈	≈	≈	≈
Sea state wave length	↑ for longer wavelengths, when wind speeds are at most moderate	↑ for shorter wavelengths, when wind speeds are at least moderate	≈	≈
Sea state Wave propagation direction	≈	↑ for wave directions parallel to the vessel's movement, if wave lengths match swell waves	↑ wave directions parallel to the vessel's movement	≈
Local Wind direction	≈	↑ for wave directions orthogonal to the vessel's movement	≈ (literature: ↑ for wave directions orthogonal to the vessel's movement, with low degree)	↑ for wave directions orthogonal to the vessel's movement
SAR slant ranges	≈	≈	↑ for shorter slant ranges	↑ for shorter slant ranges
X-band vs. C-band	≈	≈ (literature on oil: ↑ for X-band)	↑ for X-band (literature: ≈)	↑ for X-band (literature: ↓)

5. Acknowledgments:

- Data provided by the European Space Agency.
- Produced using COSMO-SkyMed satellite image © ASI (2018 - 2019), provided by e-GEOS under ESA's TPM scheme.
- RADARSAT is an official mark of the Canadian Space Agency.

6. References

[1] B. Tings, "Non-Linear Modeling of Detectability of Ship Wake Components in Dependency to Influencing Parameters Using Spaceborne X-Band SAR," *Remote Sensing,* vol. 13, no. 2, p. 165, 2021.

[2] B. Tings, A. Pleskachevsky, D. Velotto and S. Jacobsen, "Extension of Ship Wake Detectability Model for Non-Linear Influences of Parameters Using Satellite Based X-Band Synthetic Aperture Radar," *Remote Sensing,* vol. 11, no. 5, p. 563, 2019.

[3] B. Tings, A. Pleskachevsky and S. Wiehle, "Comparison of detectability of ship wake components be-tween C-Band and X-Band synthetic aperture radar sensors operating under different slant ranges," *ISPRS Journal of Photogrammetry and Remote Sensing,* vol. 196, pp. 306-324, 2023.

[4] M. D. Graziano, M. D'Errico und G. Rufino, „Wake Component Detection in X-Band SAR Images for Ship Heading and Velocity Estimation," *Remote Sensing,* Bd. 8, Nr. 6, p. 498, 2016.